Energy & Environmental Science

Cite this: *Energy Environ. Sci.*, 2012, **5**, 6453

www.rsc.org/ees

COMMUNICATION

Graphene oxide derived carbons (GODCs): synthesis and gas adsorption properties†

Gadipelli Srinivas,*[ab] Jacob Burress[a] and Taner Yildirim*[ab]

Received 11th January 2012, Accepted 7th February 2012
DOI: 10.1039/c2ee21100a

We report the synthesis of a range of high surface area graphene oxide derived carbons (GODCs) and their applications toward carbon capture and methane storage. We obtain largely increased surface areas up to nearly 1900 $m^2 g^{-1}$ for GODC samples from 10 $m^2 g^{-1}$ of precursor graphene oxide (GO). Our GODCs reveal favourable gas adsorption capacities compared to other high surface area carbons. We show that producing high surface area carbons from GO precursor is a viable method, and the porosity parameters are easily tuneable for their potential gas adsorption applications.

1. Introduction

Graphene oxide (GO) with its highly flexible layered structure and easily tuneable porous properties has been fascinating many researchers for its possible use in energy applications,[1–10] such as electrode material in electrochemical energy devices,[1–6] and gas storage, hydrogen storage and carbon capture.[7–15] In order to be applicable toward alternative energy, gas storage, and carbon capture, the material should possess high porosity and high surface area. So far, by using simple chemical methods, improved porosity and accessible surface areas are realizable from GO sheets.[1,7–15] The initial results on gas adsorption and storage in these chemically modified GO sheets are encouraging but not sufficient for large-scale industrial applications due to the limited accessible surface area and pore development. Ideally, GO sheets could display a high surface area of about 2600 $m^2 g^{-1}$, however, the experimentally obtained results are very low.[1,4,7–15] This might be due to the reordering and development of graphitic structure or retention of functional residue between graphene sheets in the chemically modified/reduced GO sheets. For instance, well-known thermal exfoliation or chemical reduction of GO leads to the development of graphitic structure, thus the reduced interlayer separation largely limits the effective molecular adsorption. In other attempts, the interlayer space between graphene sheets was developed by pillaring graphene layers using covalent functionalization or esterification of GO layer surfaces.[7,8,13,16–19] These hybrid structures pose limited porosity and surface area due to increased interlayer functional groups. As gas adsorption capacities are highly dependent on the surface area, pore structure and pore development in adsorbents, it is highly desirable that the GO sheets be processed further in new ways to obtain tailored porosity with high surface area. To approach this problem, herein we present a study on the preparation of porous carbons from the GO precursor and their application as adsorbents, especially for high pressure carbon capture and methane storage. Currently, gas adsorption by highly porous solid adsorbents is considered a very promising approach.[20–24] In this

[a]*NIST Center for Neutron Research, National Institute of Standards and Technology, Gaithersburg, Maryland, 20899-6102, USA. E-mail: taner@seas.upenn.edu; gsrinivasphys@gmail.com; Fax: +1 301-921-9847; Tel: +1 301-975-6228*
[b]*Department of Materials Science and Engineering, University of Pennsylvania, Philadelphia, Pennsylvania, 19104-6272, USA*
† Electronic supplementary information (ESI) available. See DOI: 10.1039/c2ee21100a

Broader context

Nanoporous solid adsorbents are considered one of the key materials to solve many energy and environment related problems. In particular, use of the high-capacity gas adsorption properties of these materials is a very promising approach for carbon capture and energy storage. In this study, we describe a method to obtain a wide range of highly porous carbon adsorbents through chemical activation of exfoliated graphene-oxide (exf-GO) precursors with KOH. By comparing porous properties with respect to the gas adsorption capacity of this new class of GO derived carbons (GODCs) with a range of other porous solids including activated carbons and metal–organic frameworks (MOFs), we show that our GODCs have a greater potential in gas adsorption applications. We found that the carbon dioxide and methane adsorption capacities of the porous solids maintain, approximately, a linear trend with respect to their BET surface area up to 3000 $m^2 g^{-1}$. On the other hand, the gas adsorption by MOFs seems to saturate at around 3000 $m^2 g^{-1}$, suggesting MOFs with higher surface area are not necessarily better for gas absorption applications. The results reported here clearly demonstrate that GODCs are very promising solid adsorbents for gas adsorption applications due to their easy synthesis, tunable pore size/volume, high chemical stability and low cost production.

study, various well-ordered porous activated carbon materials (we call GO derived carbons, GODCs) with a range of high surface areas were prepared through chemical activation of GO with KOH. Chemical activation is well-known for developing high porosity carbons from different carbon precursors.[25,26] We explored the effect of activation temperature and KOH concentration upon the development of porosity in resultant carbons. The detailed porous property analysis is carried out with N_2 adsorption/desorption isotherms at 77 K. The methane storage and carbon capture capacities have been estimated by measuring high pressure excess adsorption isotherms that are essential for the pressure swing adsorption process.[21] By comparing porous properties with respect to the gas storage capacity of this new class of GODCs with a range of other porous solids, we show that our GODCs have a greater potential in gas adsorption applications.

2. Experimental details

The porous GODCs were produced by chemical activation with KOH from thermally exfoliated GO (exf-GO) and solvothermally reduced GO (rGO) precursors. First, GO was synthesized by oxidizing graphite powder in a strong acidic medium using a modified Hummer's method described in detail in our earlier publications.[7,8] The, as synthesized, GO was thermally exfoliated at 250 °C under ambient air. The rGO was obtained by solvothermal synthesis at 150 °C for 48 h in methanol.[7] The GODCs were produced through two different methods of KOH activation. In the first method, exf-GO (or rGO) was thoroughly mixed with KOH in 1 : 4, 1 : 6 and 1 : 9 weight ratios using an agate mortar. The mixture was later activated at different temperatures between 600 °C and 900 °C for 60 min under N_2 atmosphere. The heating rate was controlled at around 5 °C per minute. The samples produced by this method were designated as GODC4-*T* and GODC9-*T* for 1 : 4 and 1 : 9 weight ratios of exf-GO : KOH, respectively, where *T* denotes the activation temperature. The samples were labelled as rGODC*n*-*T* in the case of the rGO precursor, here *n* is KOH to rGO ratio = 4, 6 and 9. In the second method, the exf-GO/KOH mixture was obtained through a KOH solution as described by Zhu *et al.*[6] In this method, the exf-GO (400 mg) was mixed with 20 ml KOH (7 mol) solution. This mixture was stirred for 6 h at room temperature then left soaking overnight to ensure an intimate contact of the precursor and the activator, KOH. Later, the solution was removed and the mixture was then dried at 70 °C in an oven. The dried mixture again shows approximately 9 KOH/GO,[6] more or less equal to the hand-milled method. The mixture was transferred to a horizontal quartz tube furnace for activation. The activation conditions are similar to the simple, hand-milled method. The samples produced in the solution method are denoted as GODCsol-*T*, where *T* is the activation temperature. The following steps are involved in the overall activation process: (i) constant N_2 flow was maintained throughout the whole activation process, (ii) heating the furnace to the final activation temperature of 600–900 °C at a rate of 5 °C min^{-1}, (iii) holding at the activation temperature for 60 min, and then (vi) cooling to room temperature. After the activation, all the samples were washed with distilled water until the pH value reached approximately 7. The wet samples were then dried at 100 °C overnight in air.

The GO, exf-GO, rGO and produced GODCs were characterized using powder X-ray diffraction (XRD), infrared spectroscopy (FTIR) and volumetric gas sorption analysis. XRD patterns were recorded using Cu-Kα radiation on powder samples in ambient air. FTIR spectra were collected using the KBr/sample pellet method. Before the gas sorption analysis, the samples were outgassed at 150 °C for 24 h under vacuum. The porous characteristics of the samples were obtained using nitrogen adsorption–desorption isotherms at 77 K, measured on a Quantachrome Autosorb-1-C.[27] The specific surface area was measured from the adsorption data in the relative pressure range between 0.005 and 0.05, according to the Brunauer–Emmett–Teller (BET) method. The total pore volume was estimated from the amount adsorbed at a relative pressure of 0.99. The pore size distribution was calculated from desorption branches of the isotherms using the non-local density functional theory (NLDFT) that has been applied for detailed pore size analysis. The volumetric method was used to determine the high-pressure excess adsorption–desorption isotherms at various constant temperatures.[28]

3. Results and discussion

The experimental data of powder XRD and FTIR on GO, exf-GO, rGO and produced GODCs are given in the ESI (Fig. S1 and S2†). In Fig. S1†, GO shows a single diffraction (0 0 1) peak at a 2θ of *ca.* 11.1°, corresponding to the *c*-axis interlayer distance (*d*-spacing) of 0.79 nm between GO layers. The exf-GO and rGO exhibit a weak broad (0 0 2) graphitic peak around 24.65° and 24.85°, respectively, which corresponds to a largely decreased d_{002}-spacing of around 0.36 nm. This represents a single to few layer restacked graphene sheets. The similar XRD profiles are seen for all the GODCs, which exhibit further very weak, broad peaks compared to exf-GO, centered around 26° and 44°, the reflection from graphitic (0 0 2) and (1 0 0) planes, respectively. The d_{002} is around 0.34 nm, close to that of graphite (0.335 nm). The increased low-angle scattering in GODCs might be due to the presence of high porosity.[6] Fig. S2† shows the FTIR spectra of precursor GO, exf-GO and GODCs. The FTIR spectrum of GO showed a few vibrational bands at *ca.* 3410 cm^{-1} due to hydroxyl stretching vibrations in COOH and/or intercalated water, 1720 cm^{-1} due to the C=O stretching vibration of the carboxyl group, 1630 cm^{-1} owing to aromatic C=C, 1380 cm^{-1} due to O–H bending from hydroxyl/phenol groups and 1053 cm^{-1} due to alkoxy C–O stretching vibrations.[7] The exf-GO, rGO and GODCs show considerably reduced or missing oxygen-containing groups: C=O, C–O and hydroxyl/phenol bonds suggesting a considerable de-oxygenation. A band at about 1557 cm^{-1} due to skeletal vibration is seen in exf-GO. The vibrational bands (at *ca.* 3410 cm^{-1}) present in these samples are likely due to moisture adsorption from air before the measurements.

The porosity characteristics of the samples were investigated by measuring the N_2 adsorption–desorption isotherms at 77 K and are shown in Fig. 1, S3 and S4†. The corresponding pore size distributions of the samples are shown in Fig. 2. The negligible N_2 adsorption in GO and rGO is indicative of the filled interlayer galleries in GO and the restacked graphitic structure in rGO. The exf-GO shows a continuous increase in N_2 uptake and also exhibits a large hysteresis at relative pressure above 0.5, which indicates the presence of mesopores. In contrast, all the GODCs exhibit a relatively high adsorption. The major uptake occurs at a relatively low pressure, indicating the formation of highly microporous materials. With increasing activation temperature and/or KOH concentration the samples gain pore volume in mesopores. The samples display the hysteresis effect and slope of the plateau with a significant increase in the nitrogen

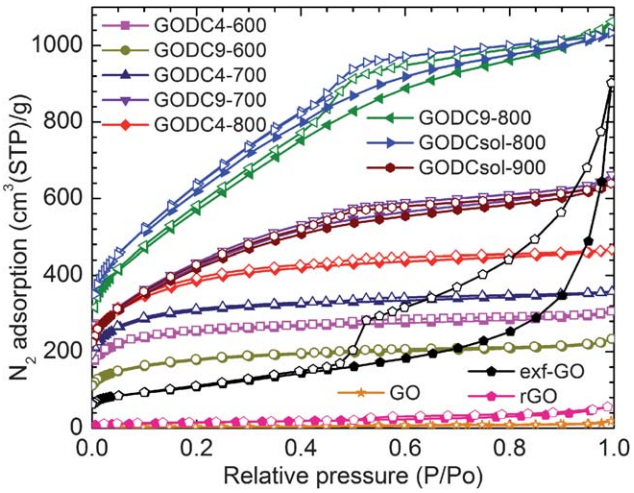

Fig. 1 N_2 adsorption–desorption isotherms of GO, rGO, exf-GO and GODCs produced under different activation conditions, measured at 77 K. The solid and open data points represent adsorption and desorption isotherms respectively.

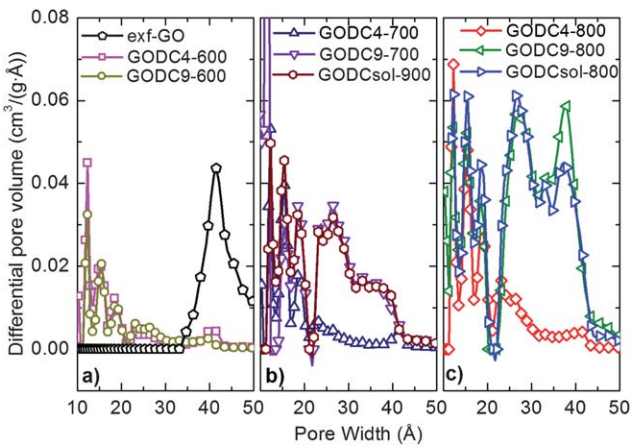

Fig. 2 Pore size distribution of exf-GO and GODCs produced under different activation conditions. The data are derived from the N_2 adsorption isotherms shown in Fig. 1.

uptake through the entire pressure range. Analysis of the isotherms indicates that the main differences between the samples are development in their pore volumes and their pore size distribution. The porosity parameters obtained from N_2 adsorption isotherms of the samples are summarized in Table 1. In terms of pore size distribution (Fig. 2), the exf-GO shows only mesoporosity. However, the GODC samples at low activation temperature and KOH concentrations (GODC4-600, GODC9-600 and GODC4-700) show a pore development in the microporous region, while increasing the activation temperature and KOH concentration (GODC9-700, GODC9-800, GODCsol-800) results in a large proportion of pore development in both the microporous and mesoporous regions (>2 nm). The low temperature and/or low KOH concentration activated samples show BET surface area and pore volume between 600 $m^2\ g^{-1}$ and 1300 $m^2\ g^{-1}$, and 0.36 $cm^3\ g^{-1}$ and 0.72 $cm^3\ g^{-1}$, respectively, with dominant microporosity with an average pore size around 1.5 nm. Under rigorous activation conditions (high activation temperature and/or high KOH concentrations) the samples exhibit high specific surface area between 1300 $m^2\ g^{-1}$ and 1900 $m^2\ g^{-1}$ and high pore volume between 1.00 $cm^3\ g^{-1}$ and 1.65 $cm^3\ g^{-1}$ with an average pore size around 2.5 nm. The effect of activation temperature and KOH concentration on BET surface area is compared in Fig. S5† for all the samples. It can be seen that the optimal conditions to obtain the highest BET surface area and pore volumes are 800 °C and 1 : 9 GO/KOH, which is in good agreement with Zhu *et al.*[6] The low temperature is not favourable to increase porosity due to the slow reaction rate between the activator, KOH and exf-GO. This might be the reason for producing a lower surface area in sample GODC9-600 than GODC4-600. The high temperature activation probably damages the pores formed at the previous stage, thus samples activated at 900 °C show poor pore development. The exf-GO exhibits a high pore volume of 1.4 $cm^3\ g^{-1}$ and a pore size of 0.40 nm due to the highly wrinkled nature of single to few layer graphene sheets. The highly decreased pore size of the GODCs compared to that of the exf-GO is caused by the severe shrinkage and restructuring of the wrinkled graphenes. From the analysis it is very clear that the activation temperature and KOH concentration play a critical role in determining the specific surface area and pore volume of the resultant carbons. The pore structures with high surface area can be developed by rigorous evolution of gaseous by-products during KOH activation. According to the chemical activation mechanism,[26] it is suggested that during the activation, the chemical reaction between KOH and carbons proceeds as $6KOH + C = 2K + 3H_2 + 2K_2CO_3$, followed by either decomposition of K_2CO_3 or reaction of $K/K_2CO_3/CO_2$ with carbon. Thus with increasing activation temperature and KOH concentration, simultaneous pore opening and pore widening are observed. Above the optimum activation temperature, 900 °C, the samples show decreased surface area and pore volume due to further reaction of the porous carbon, thus the samples produced at this temperature also have very low yield.

It is important to note that from Fig. S4† the rGODCs exhibit significantly reduced pore development when compared to the GODCs for the similar activation conditions. The maximum BET surface area ~920 $m^2\ g^{-1}$ of rGODC9-800 is far less than ~1700 $m^2\ g^{-1}$ of GODC9-800. This explains the importance of the type of initial GO used in obtaining highly porous carbons. It is very often the precursor carbon that is the key to obtaining higher surface areas. In general, porous carbon materials consist of randomly oriented defective graphite nanoflakes, and the thickness of the graphite nanoflakes can determine the SSA of the products. Thus the restacked graphene layers in rGO might be the reason the resultant carbons exhibit a lower surface area. It is also worthy to note that our GODCsol-800 sample made with the Zhu *et al.* method exhibits less surface area, ~1900 $m^2\ g^{-1}$ than ~2500 $m^2\ g^{-1}$ reported in ref. 6. This can be attributed to the extent that the GO is exfoliated.

The high pressure CO_2 adsorption excess isotherms at 300 K for all the samples are shown in Fig. 3. It can be seen that the samples with highest BET surface area show highest adsorption. The slope of the isotherms is also comparatively similar to the N_2 adsorption isotherms, where the BET surface area, pore volume, and pore size distribution play major roles in the high pressure adsorption behaviour of the isotherms. Fig. S6† represents the CO_2 adsorption isotherms of the samples up to 1 bar. The adsorption capacity *versus* BET surface area, total pore volume and average pore size is plotted in Fig. 4. It is observed that the high pressure CO_2 adsorption trend is more or less linearly dependent on the BET surface area, total pore

Table 1 GODCs with synthesis conditions (KOH/exf-GO concentration and activation temperature), yield by weight of precursor exf-GO, the porosity parameters: BET surface area, average pore size, porosity based on a skeleton density of 2 g cm^{-3}, and high pressure CO_2 and methane adsorption capacities at 20 bar and 35 bar, respectively, at 300 K

Sample	Yield by weight (%)	BET surface area/m^2 g^{-1}	Total pore volume/cm^3 g^{-1}	Average pore size/nm	Porosity (%)	CO_2 adsorption/ mg mg^{-1}	Methane adsorption/ mg mg^{-1}
GODC4-600	54	916	0.48	1.30	49	0.390	0.096
GODC9-600	36	619	0.36	1.54	42	0.360	0.084
GODC4-700	53	1096	0.56	1.54	53	0.480	0.119
GODC9-700	28	1326	1.10	1.85	69	0.555	0.137
GODC4-800	38	1276	0.72	1.60	59	0.497	0.126
GODC9-800	26	1704	1.65	2.60	77	0.652	0.163
GODCsol-800	33	1894	1.60	2.40	76	0.721	0.175
GODCsol-900	10	1272	0.99	1.86	66	0.525	0.137

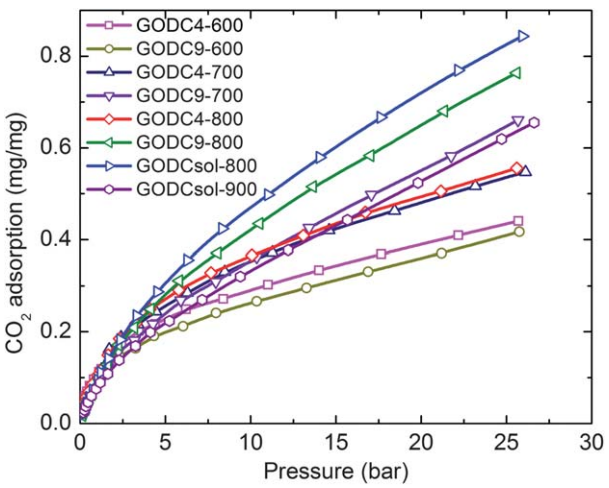

Fig. 3 The room temperature (300 K) CO_2 excess adsorption isotherms of GODCs produced under different activation conditions.

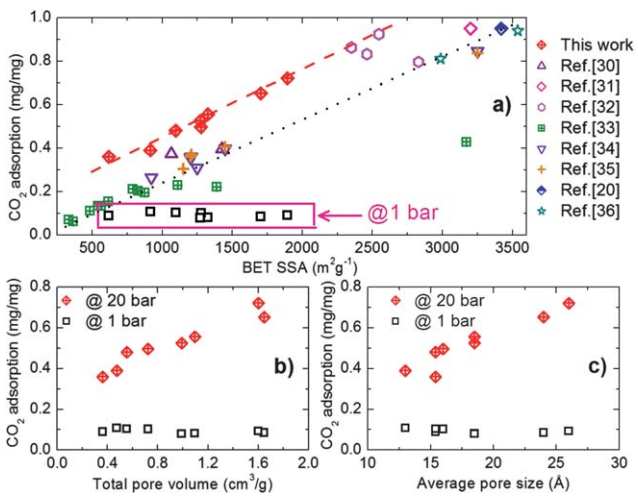

Fig. 4 The low pressure (1 bar) and high pressure (20 bar) CO_2 adsorption capacities at 300 K with respect to the BET surface area (a), total pore volume (b) and average pore size (c). Around room temperature (298–300 K) the CO_2 adsorption capacities at 20 bar of our GODCs and a range of other porous carbons are compared with respect to the most important porosity parameter, BET surface area, that defines the adsorption capacities of most of the porous solids (a) (ref. 35). "+" represents the commercial activated carbons.

volume, and average pore size. The low pressure (~1 bar) adsorption behaviour is almost independent of the surface area similar to the most of porous carbons.[29] The narrow pore size distribution in the micropore region appears to produce better uptake values at 1 bar but these isotherms tend to saturate at low to moderate pressures due to pore filling. The high pressure isotherms show improved adsorption capacities over other activated carbons.[20,21,29–35] For instance, Fig. 4a and S7† compare the high pressure CO_2 adsorption capacities of our GODC samples with a range of other high surface area carbons. Our GODC samples definitely show improved adsorption capacities for CO_2 storage. It can be observed that a general trend exists for all the materials, the higher the surface area, the higher the adsorption capacity. Only amine functionalized or microwave irradiated carbons can reach the storage capacity of GODCs.[32]

Fig. 5 shows the high-pressure methane excess adsorption isotherms of GODCs at 300 K. Fig. S8† represents the low pressure methane adsorption isotherms of the samples up to 1 bar. The adsorption capacity against the BET surface area, total pore volume and average pore size is plotted in Fig. 6. Similar to CO_2 adsorption, methane adsorption capacities increase with porous parameters. With respect to the BET surface area, again the improved performance in high pressure methane uptake is seen in our GODCs compared to most of the other porous carbons[30,35–42] (Fig. 6a). The high adsorption capacities of our GODCs can be directly related to

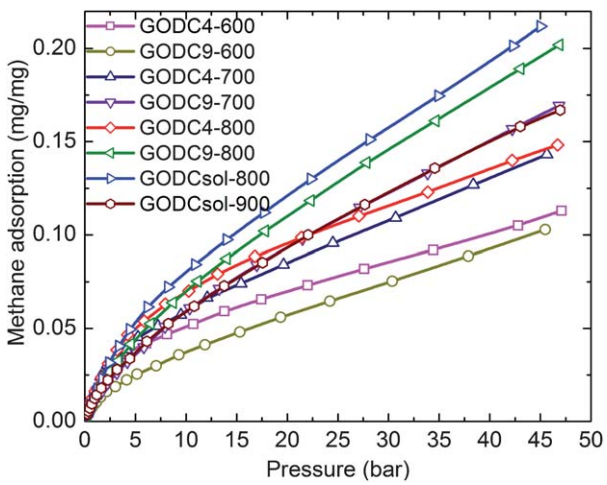

Fig. 5 The room temperature (300 K) methane excess adsorption isotherms of GODCs produced under different activation conditions.

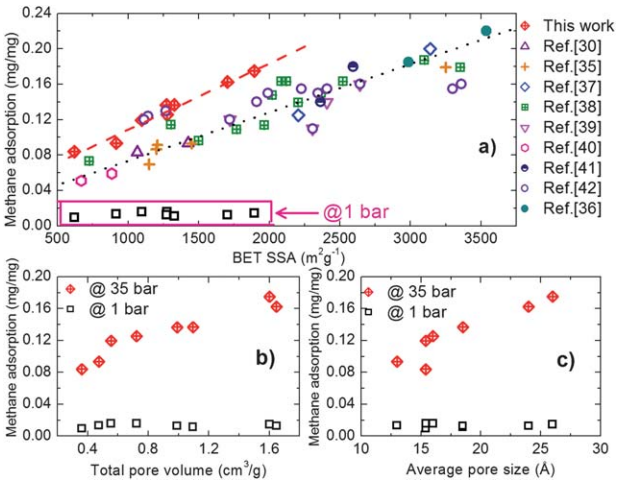

Fig. 6 The low pressure (1 bar) and high pressure (35 bar) methane adsorption capacities at 300 K with respect to the BET surface area (a), total pore volume (b) and average pore size (c). Around room temperature (298–300 K) the methane adsorption capacities at 35 bar of our GODCs and a range of other porous carbons are compared with respect to the BET surface area (a) (ref. 35). "+" represents the commercial activated carbons.

the hierarchical pore structure with large pore volume. At moderate surface area (<1500 $m^2\ g^{-1}$), GODCs and activated carbide derived carbons[42] show similar methane adsorption capacities due to the very narrow pore size distribution in the micropore range. Fig. S9 and S10† compare the carbon dioxide and methane high pressure adsorption isotherms of GODCs and commercial Maxsorb and Norit R1 carbons. It is worthy to note that from the given surface areas, our GODC samples perform better in gas adsorption applications.

We further compared the CO_2 and methane adsorption capacities of GODCs with other porous coordinated framework materials. Fig. 7 represents the comparison of high-pressure CO_2 and methane adsorption capacities of GODCs, metal–organic frameworks (MOFs)[23,43–49] and covalent–organic frameworks (COFs)[24] against their BET surface area. The organic frameworks are well-known for their large surface areas, wide pore structures, and versatile chemical compositions. They are widely investigated for their possible usage toward alternative energy, gas storage applications and carbon capture. On comparing with respect to the surface area, from Fig. 7 it is very clear that none of these MOFs surpass the CO_2 and methane adsorption capacities of the GODCs at given pressures. It is worthy to note that from the comparison of CO_2 and methane adsorption capacities of the porous solids with respect to their BET surface area, one can estimate the adsorption capacities based on the BET surface area only up to a certain limit around 3000 $m^2\ g^{-1}$, below this limit most of the solids exhibit a more or less linear trend between high pressure adsorption capacity and BET surface area. Only some of the MOFs exhibit comparable CO_2 and methane uptake capacities to those of GODCs in the limited surface areas up to about 3000 $m^2\ g^{-1}$. Even though some of the MOFs exhibit very high surface areas up to over 6000 $m^2\ g^{-1}$, their gas adsorption capacities appear not to be significantly better than the solids with surface areas around 3000 $m^2\ g^{-1}$. This might be due to the existence of very large pore sizes that are not effectively providing further increase in gas adsorption

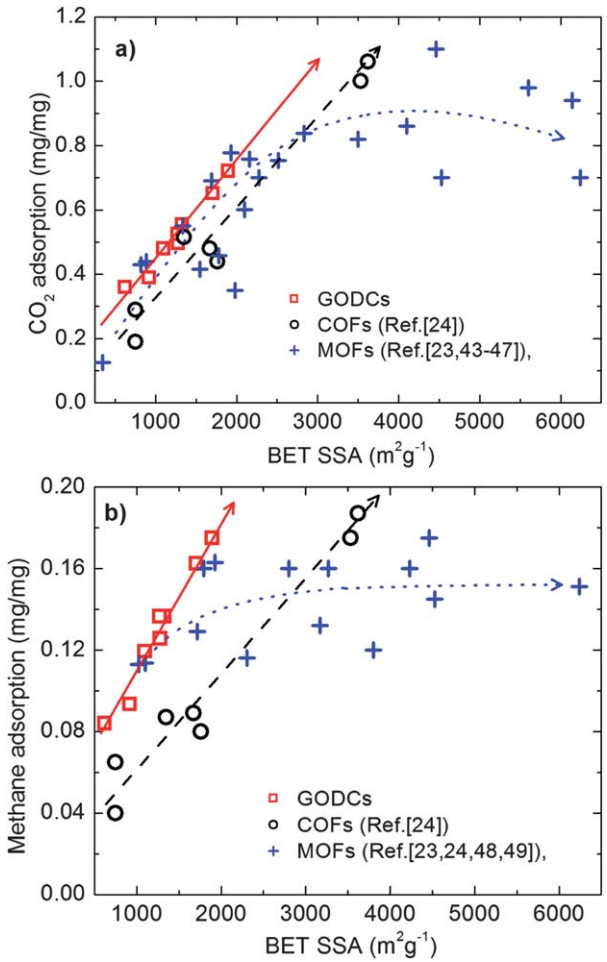

Fig. 7 The room temperature (298–300 K) and high pressure CO_2 (a) and methane (b) adsorption capacities at 20 bar and 35 bar, respectively, of our GODCs and a range of other porous organic frameworks compared with respect to the BET surface area.

capacities. Thus targeting ultra-high surface area materials may not be a key factor for optimum gas adsorption. Nevertheless some of the MOFs exhibit very good carbon dioxide and methane adsorption capacities under ambient conditions compared to known porous carbons. Additionally, the chemical stability of these organic frameworks, that is whether these solids maintain their structural integrity and function when subjected to the harsh environment of combustion gases, is under debate.[22,23,50,51] Flue gas, containing moisture and acid gases (SO_x and NO_x), may lead to the degradation of the framework stability.[22,23,50,51] In addition, most of these solids developed through expanded links, which often yield fragile frameworks, and self-interpenetration thereby losing accessible surface area. Therefore, it is important for the potential adsorbents to be stable in the presence of acid gases. In this regard, porous carbon materials with the rigid pores, good chemical resistance, high surface areas and tuneable pore volume could play a promising role as high pressure adsorbents.[51,52] The other advantage is that the costs associated to produce porous carbons are low and they are easily synthesized in mass quantities with tailored pore structure by simply controlling the activation conditions (KOH/GO concentration and temperature). Finally, GODCs also exhibit a sufficiently moderate heat of adsorption

(Fig. S11 to S14†) to play a useful role in large-scale, reversible carbon capture. Thus these combined properties of GODCs can be conveniently used in pressure swing adsorption. It is a promising process that could be applied immediately for the removal of CO_2 from industrial point sources because it is energy efficient and suitable for a large-scale CO_2 capture system.[21]

4. Conclusions

We report the synthesis of high surface area porous carbons from graphene oxide precursor with KOH chemical activation. The optimum activation condition is found to be 800 °C and 1 : 9 GO to KOH ratio to obtain a porous carbon with a highest BET surface area of 1900 $m^2 g^{-1}$ and the maximum total pore volume of 1.65 $cm^3 g^{-1}$. We have shown that the specific surface area, pore volume and pore size distribution are tuneable with KOH concentration and activation temperature. GODCs with hierarchical pore structure have the potential for carbon dioxide and methane adsorption applications. In addition, these carbons also exhibit a sufficiently low heat of adsorption to play a useful role in large-scale, reversible gas adsorption. The observed results clearly demonstrate that GO could become a reliable route to prepare a highly porous carbon material with high surface area and tailored micro/mesopores which would play an important role in obtaining high adsorption capacities for industrial use.

Acknowledgements

This work was supported by DOE BES grant no. DE-FG02-08ER46522.

Notes and references

1 Y. Sun, Q. Wu and G. Shi, Graphene based new energy materials, *Energy Environ. Sci.*, 2011, **4**, 1113–1132.
2 O. C. Compton and S. T. Nguyen, Graphene oxide, highly reduced graphene oxide, and graphene: versatile building blocks for carbon-based materials, *Small*, 2010, **6**, 711–723.
3 G. Eda and M. Chhowalla, Chemically derived graphene oxide: towards large-area thin-film electronics and optoelectronics, *Adv. Mater.*, 2010, **22**, 2392–2415.
4 Y. Zhu, S. Murali, W. Cai, X. Li, J. W. Suk, J. R. Potts and R. S. Ruoff, Graphene and graphene oxide: synthesis, properties, and applications, *Adv. Mater.*, 2010, **22**, 3906–3924.
5 M. Segal, Selling graphene by the ton, *Nat. Nanotechnol.*, 2009, **4**, 612–614.
6 Y. Zhu, S. Murali, M. D. Stoller, K. J. Ganesh, W. Cai, P. J. Ferreira, A. Pirkle, R. M. Wallace, K. A. Cychosz, M. Thommes, D. Su, E. A. Stach and R. S. Ruoff, Carbon-based supercapacitors produced by activation of graphene, *Science*, 2011, **332**, 1537–1541.
7 G. Srinivas, J. W. Burress, J. Ford and T. Yildirim, Porous graphene oxide frameworks: synthesis and gas sorption properties, *J. Mater. Chem.*, 2011, **21**, 11323–11329.
8 J. W. Burress, S. Gadipelli, J. Ford, J. M. Simmons, W. Zhou and T. Yildirim, Graphene oxide framework materials: theoretical predictions and experimental results, *Angew. Chem., Int. Ed.*, 2010, **49**, 8902–8904.
9 G. Srinivas, Y. Zhu, R. Piner, N. Skipper, M. Ellerby and R. Ruoff, Synthesis of graphene-like nanosheets and their hydrogen adsorption capacity, *Carbon*, 2010, **48**, 630–635.
10 A. Ghosh, K. S. Subrahmanyam, K. S. Krishna, S. Datta, A. Govindaraj, S. K. Pati and C. N. R. Rao, Uptake of H_2 and CO_2 by graphene, *J. Phys. Chem. C*, 2008, **112**, 15704–15707.
11 L. P. Ma, Z. S. Wu, J. Li, E. D. Wu, W. C. Ren and H. M. Cheng, Hydrogen adsorption behavior of graphene above critical temperature, *Int. J. Hydrogen Energy*, 2009, **34**, 2329–2332.
12 Z.-L. Hu, M. Aizawa, Z.-M. Wang, N. Yoshizawa and H. Hatori, Synthesis and characteristics of graphene oxide-derived carbon nanosheet-Pd nanosized particle composites, *Langmuir*, 2010, **26**, 6681–6688.
13 G. K. Dimitrakakis, E. Tylianakis and G. E. Froudakis, Pillared graphene: a new 3-D network nanostructure for enhanced hydrogen storage, *Nano Lett.*, 2008, **8**, 3166–3170.
14 D. Long, W. Li, L. Ling, J. Miyawaki, I. Mochida and S.-H. Yoon, Preparation of nitrogen-doped graphene sheets by a combined chemical and hydrothermal reduction of graphene oxide, *Langmuir*, 2010, **26**, 16096–16102.
15 D. Zhou and B.-H. Han, Graphene-based nanoporous materials assembled by mediation of polyoxometalate nanoparticles, *Adv. Funct. Mater.*, 2010, **20**, 2717–2722.
16 H. J. Salavagione, M. A. Gómez and G. Martínez, Polymeric modification of graphene through esterification of graphite oxide and poly(vinyl alcohol), *Macromolecules*, 2009, **42**, 6331–6334.
17 K. W. Putz, O. C. Compton, M. J. Palmeri, S. T. Nguyen and L. C. Brinson, High-nanofiller-content graphene oxide–polymer nanocomposites *via* vacuum-assisted self-assembly, *Adv. Funct. Mater.*, 2010, **20**, 3322–3329.
18 D.-D. Zhang, S.-Z. Zu and B.-H. Han, Inorganic–organic hybrid porous materials based on graphite oxide sheets, *Carbon*, 2009, **47**, 2993–3000.
19 M. Herrera-Alonso, A. A. Abdala, M. J. McAllister, I. A. Aksay and R. K. Prud'homme, Intercalation and stitching of graphite oxide with diaminoalkanes, *Langmuir*, 2007, **23**, 10644–10649.
20 S. Builes, T. Roussel, C. M. Ghimbeu, J. Parmentier, R. Gadiou, C. Vix-Guterl and L. F. Vega, Microporous carbon adsorbents with high CO_2 capacities for industrial applications, *Phys. Chem. Chem. Phys.*, 2011, **13**, 16063–16070.
21 M. T. Ho, G. W. Allinson and D. E. Wiley, Reducing the cost of CO_2 capture from flue gases using pressure swing adsorption, *Ind. Eng. Chem. Res.*, 2008, **47**, 4883–4890.
22 C. Lastoskie, Caging carbon dioxide, *Science*, 2010, **330**, 595–596.
23 H. Furukawa, N. Ko, Y. B. Go, N. Aratani, S. B. Choi, E. Choi, A. Ö. Yazaydin, R. Q. Snurr, M. O'Keeffe, J. Kim and O. M. Yaghi, Ultrahigh porosity in metal–organic frameworks, *Science*, 2010, **329**, 424–428.
24 H. Furukawa and O. M. Yaghi, Storage of hydrogen, methane, and carbon dioxide in highly porous covalent organic frameworks for clean energy applications, *J. Am. Chem. Soc.*, 2009, **131**, 8875–8883.
25 H. Marsh and F. Rodríguez-Reinoso, *Activated Carbon*, Elsevier, London, 2006.
26 M. A. Lillo-Ródenas, D. Cazorla-Amorós and A. Linares-Solano, Understanding chemical reactions between carbons and NaOH and KOH: an insight into the chemical activation mechanism, *Carbon*, 2003, **41**, 267–275.
27 Certain trade names and company products are mentioned in this paper to adequately specify the experimental procedure and equipment used. In no case does this imply recommendation or endorsement by NIST, nor does it imply that the products are necessarily the best available for this purpose.
28 W. Zhou, H. Wu, M. R. Hartman and T. Yildirim, Hydrogen and methane adsorption in metal–organic frameworks: a high-pressure volumetric study, *J. Phys. Chem. C*, 2007, **111**, 16131–16137.
29 X. Hu, M. Radosz, K. A. Cychosz and M. Thommes, CO_2-filling capacity and selectivity of carbon nanopores: synthesis, texture, and pore-size distribution from quenched-solid density functional theory (QSDFT), *Environ. Sci. Technol.*, 2011, **45**, 7068–7074.
30 Y. Sun and P. A. Webley, Preparation of activated carbons with large specific surface areas from biomass corncob and their adsorption equilibrium for methane, carbon dioxide, nitrogen, and hydrogen, *Ind. Eng. Chem. Res.*, 2011, **50**, 9286–9294.
31 B. B. Saha, S. Jribi, S. Koyama and I. I. El-Sharkawy, Carbon dioxide adsorption isotherms on activated carbons, *J. Chem. Eng. Data*, 2011, **56**, 1974–1981.
32 Z. Zhang, M. Xu, H. Wang and Z. Li, Enhancement of CO_2 adsorption on high surface area activated carbon modified by N_2, H_2 and ammonia, *Chem. Eng. J.*, 2010, **160**, 571–577.
33 T. C. Drage, J. M. Blackman, C. Pevida and C. E. Snape, Evaluation of activated carbon adsorbents for CO_2 capture in gasification, *Energy Fuels*, 2009, **23**, 2790–2796.
34 B. Mu and K. S. Walton, High-pressure adsorption equilibrium of CO_2, CH_4, and CO on an impregnated activated carbon, *J. Chem. Eng. Data*, 2011, **56**, 390–397.

35 S. Himeno, T. Komatsu and S. Fujita, High-pressure adsorption equilibria of methane and carbon dioxide on several activated carbons, *J. Chem. Eng. Data*, 2005, **50**, 369–376.
36 X. Shao, Z. Feng, R. Xue, C. Ma, W. Wang, X. Peng and D. Cao, Adsorption of CO_2, CH_4, CO_2/N_2 and CO_2/CH_4 in novel activated carbon beads: preparation, measurements and simulation, *AIChE J.*, 2011, **57**, 3042–3051.
37 W. S. Loh, K. A. Rahman, A. Chakraborty, B. B. Saha, Y. S. Choo, B. C. Khoo and K. C. Ng, Improved isotherm data for adsorption of methane on activated carbons, *J. Chem. Eng. Data*, 2010, **55**, 2840–2847.
38 D. Lozano-Castello, D. Cazorla-Amoros and A. Linares-Solano, Powdered activated carbons and activated carbon fibers for methane storage: a comparative study, *Energy Fuels*, 2002, **16**, 1321–1328.
39 M. Sevillaab and R. Mokaya, Activation of carbide-derived carbons: a route to materials with enhanced gas and energy storage properties, *J. Mater. Chem.*, 2011, **21**, 4727–4732.
40 A. Martin, W. S. Loh, K. A. Rahman, K. Thu, B. Surayawan, M. I. Alhamid, Nasruddin and K. C. Ng, Adsorption isotherms of CH_4 on activated carbon from Indonesian low grade coal, *J. Chem. Eng. Data*, 2011, **56**, 361–367.
41 C. Vakifahmetoglu, V. Presser, S.-H. Yeon, P. Colombo and Y. Gogotsi, Enhanced hydrogen and methane gas storage of silicon oxycarbide derived carbon, *Microporous Mesoporous Mater.*, 2011, **144**, 105–112.
42 S.-H. Yeona, S. Osswalda, Y. Gogotsi, J. P. Singerb, J. M. Simmons, J. E. Fischer, M. A. Lillo-Ródenasd and Á. Linares-Solano, Enhanced methane storage of chemically and physically activated carbide-derived carbon, *J. Power Sources*, 2009, **191**, 560–567.
43 J. M. Simmons, H. Wu, W. Zhou and T. Yildirim, Carbon capture in metal–organic frameworks-a comparative study, *Energy Environ. Sci.*, 2011, **4**, 2177–2185.
44 A. R. Millward and O. M. Yaghi, Metal–organic frameworks with exceptionally high capacity for storage of carbon dioxide at room temperature, *J. Am. Chem. Soc.*, 2005, **127**, 17998–17999.
45 B. Mu, P. M. Schoenecker and K. S. Walton, Gas adsorption study on mesoporous metal–organic framework UMCM-1, *J. Phys. Chem. C*, 2010, **114**, 6464–6471.
46 O. K. Farha, A. O. Yazaydın, I. Eryazici, C. D. Malliakas, B. G. Hauser, M. G. Kanatzidis, S. T. Nguyen, R. Q. Snurr and J. T. Hupp, De novo synthesis of a metal–organic framework material featuring ultrahigh surface area and gas storage capacities, *Nat. Chem.*, 2010, **2**, 944–948.
47 T. Ben, H. Ren, S. Ma, D. Cao, J. Lan, X. Jing, W. Wang, J. Xu, F. Deng, J. M. Simmons, S. Qiu and G. Zhu, Targeted synthesis of a porous aromatic framework with high stability and exceptionally high surface area, *Angew. Chem., Int. Ed.*, 2009, **48**, 9457–9460.
48 W. Zhou, Methane storage in porous metal–organic frameworks: current records and future perspectives, *Chem. Rec.*, 2010, **10**, 200–204.
49 J. Y. Lee, L. Pan, X. Huang, T. J. Emge and J. Li, A systematic approach to building highly porous, noninterpenetrating metal–organic frameworks with a large capacity for adsorbing H_2 and CH_4, *Adv. Funct. Mater.*, 2011, **21**, 993–998.
50 J. Liu, A. I. Benin, A. M. B. Furtado, P. Jakubczak, R. R. Willis and M. D. LeVan, Stability effects on CO_2 adsorption for the DOBDC series of metal–organic frameworks, *Langmuir*, 2011, **27**, 11451–11456.
51 J. R. Holst and A. I. Cooper, Ultrahigh surface area in porous solids, *Adv. Mater.*, 2010, **22**, 5212–5216.
52 V. Presser, J. McDonough, S.-H. Yeon and Y. Gogotsi, Effect of pore size on carbon dioxide sorption by carbide derived carbon, *Energy Environ. Sci.*, 2011, **4**, 3059–3066.